

Marangoni Flow of Soluble Amphiphiles

Matthieu Roché,^{1,†} Zhenzhen Li,^{1,‡} Ian M. Griffiths,² Sébastien Le Roux,³ Isabelle Cantat,³
Arnaud Saint-Jalmes,³ and Howard A. Stone^{1,*}

¹*Department of Mechanical and Aerospace Engineering, Princeton University, Princeton, New Jersey 08544, USA*

²*Mathematical Institute, University of Oxford, Oxford OX2 6GG, United Kingdom*

³*Institut de Physique de Rennes, CNRS UMR 6251, Université Rennes 1, 35042 Rennes, France*

(Received 4 December 2013; revised manuscript received 19 February 2014; published 20 May 2014)

Surfactant distribution heterogeneities at a fluid-fluid interface trigger the Marangoni effect, i.e., a bulk flow due to a surface tension gradient. The influence of surfactant solubility in the bulk on these flows remains incompletely characterized. Here we study Marangoni flows sustained by injection of hydro-soluble surfactants at the air-water interface. We show that these flows have a finite size that increases with a decrease of the critical micelle concentration of the surfactants. We document the universality of the surface velocity field of these finite flows and predict scaling laws based on hydrodynamics and surfactant physical chemistry that capture the flow features.

DOI: 10.1103/PhysRevLett.112.208302

PACS numbers: 82.70.Uv, 47.55.dk, 47.55.pf

The release of a drop of water mixed with dishwashing liquid on the surface of pure water covered with pepper grains demonstrates the Marangoni effect [1]: after the drop touches the water surface, pepper grains are transported to the edge of the bowl (movie M1 in the Supplemental Material [34]). The flow results from a surface tension difference between water at the point of release and clean water far away. The Marangoni effect plays an important role in many natural and industrial processes such as pulmonary surfactant replacement therapy [2,3], motion and defense of living organisms [4–6], emulsion and foam stability [7,8], and many others [9–12]. In these settings, surfactants generally have a finite solubility in one of the phases, but the effect of interface-bulk mass exchange on Marangoni flows is still not understood despite its consequences on flow (Movie M2 in Supplemental Material [34]). Most studies [13–16] have focused on the deposition of droplets of surfactant solutions on thin films, but the transient nature of the induced flow and the small size of the film prevented the validation of proposed descriptions.

Here, we investigate axisymmetric continuous Marangoni flows induced by hydrosoluble surfactants on centimeter-thick water layers. We document the spatial structure of these flows. We show how the rapid Marangoni flow is limited to a finite area on the water surface, which we call the transparent zone, whose extent and velocity field depend on the surfactant chemical structure, hence on amphiphile thermodynamic properties such as the critical micelle concentration (cmc). We propose scaling laws based on hydrodynamics and physical chemistry for the radius and velocity in the transparent zone, which are in excellent agreement with the experiments.

We characterized the Marangoni flow of water induced by hydrosoluble amphiphiles using eight surfactants from the alkyl trimethylammonium halides (C_n TAB, $n = 10$

to 14; C_n TAC, $n = 12$ and 16), and the sodium alkyl sulfate (C_n NaSO₄, $n = 8$ to 12) families (Sigma-Aldrich, purity 99%), whose critical micelle concentration vary over 2 orders of magnitude [17–23] (see Table 1 in the Supplemental Material [34]). Surfactant solutions, seeded with light-scattering 10- μ m olive oil droplets, were supplied on the surface of an ultrapure water layer (Millipore Q, resistivity $\sigma = 18.2$ M Ω -cm) using a syringe pump (Harvard Apparatus PHD2000) at a constant surfactant molar flow rate $Q_a = \theta Qc$, with $\theta = V_s/(V_s + V_{oil})$ the volume fraction of surfactant solution in the injected liquid, V_s and V_{oil} the volumes of surfactant solution and oil used to prepare the injected solution, Q the total volume flow rate, and c the surfactant concentration [Fig. 1(a)]. We checked that oil droplets acted as passive tracers (i.e., their Stokes number is small) and did not influence flow properties (Fig. S1 in the Supplemental Material [34], and discussion therein). This setup is similar to the one used in previous studies of the Marangoni flow of completely or partially hydrosoluble liquids on water [24–26].

The flow is divided into three regions [Fig. 1(b) and movie M3 in the Supplemental Material [34]]. A zone of significant light scattering, the source, surrounds the injection point, over distance r_s . Further downstream, we observe a region of radius r_t of little scattered light that we call the transparent zone. Outside the transparent zone, intense light scattering is observed again, and vortex pairs similar to those reported in the case of thermocapillary Marangoni flows [27] grow along the air-water interface and expand outwards. Further from the source, the tracers move only slightly, suggesting that surface tension is spatially homogeneous in this region and that the Marangoni flow is located in the transparent region. A side view of the experiment reveals the existence of a three-dimensional recirculating flow in the bulk fluid

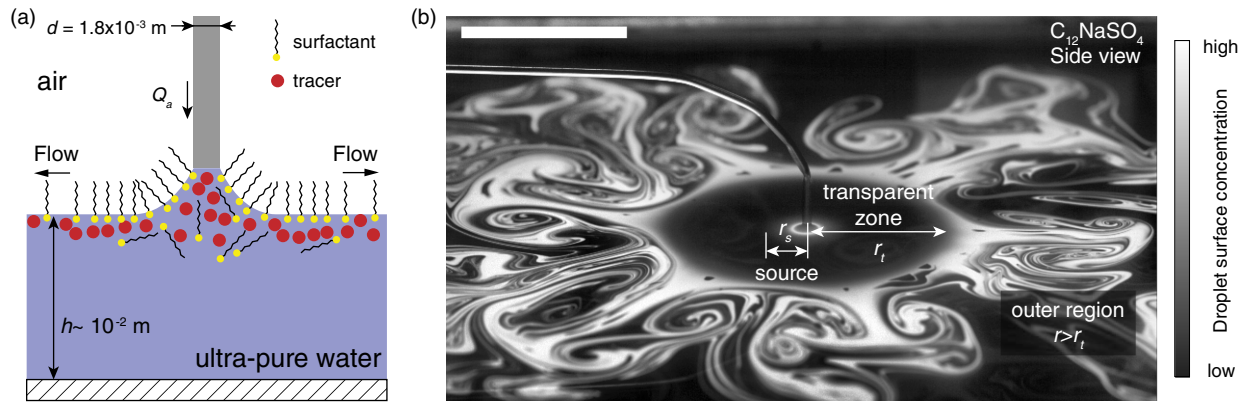


FIG. 1 (color online). Experimental observation of the Marangoni flow. (a) Schematic of the experimental setup in the region surrounding the point of injection. (b) Side view of a typical experiment. In this view, regions of high coverage in light-scattering tracers are white. The different flow regions (source, transparent zone, and outer region) are identified on the picture. Surfactant molar flow rate $Q_a = 0.52 \times 10^{-6} \text{ mol} \cdot \text{s}^{-1}$, scale bar: $3 \times 10^{-2} \text{ m}$.

below the transparent zone, which changes direction at $r = r_t$ and then follows the bottom of the container back towards the source. Similar results have been reported in the case where surfactants had accumulated on the water surface [28,29]. We note here that our measurements are performed at times when bulk surfactant concentration in the water layer is at most a few thousandths of the critical micelle concentration. We checked that the surface pressure of water outside the transparent zone remained equal to zero during our measurements. Hence, our observations result from another mechanism other than surfactant accumulation.

The size of the different flow regions depends on the surfactant molecular structure. We observed that, for a constant molar flow rate Q_a , the radius of the transparent zone r_t varies over almost 2 orders of magnitude when n increases twofold [Fig. 2(a)]. Also, r_t depends on the properties of the surfactant polar headgroup, in particular, on its effective radius r_{eff} , which accounts for electrostatic and ion-specific effects [30,31]. For example, an increase of r_{eff} by using $\text{C}_{12}\text{NaSO}_4$ instead of C_{12}TAB results in a decrease of r_t .

The radius of the transparent zone r_t also varies with time [Fig. 2(a)]. After an initial increase, r_t remains constant at a maximal value $r_{t,\text{max}}$ for a time dependent on finite-size effects due to the container (Fig. S2 in Supplemental Material [34]). Then, r_t decreases slowly, before a sharp decrease is observed at longer times, corresponding to a significant increase of the surfactant concentration in the water layer (Fig. S3 in Supplemental Material [34]).

The relationship between Q_a and $r_{t,\text{max}}$ is nonlinear [Fig. 2(b)] in contrast with the linear dependence between $r_{t,\text{max}}$ and Q_a reported in earlier studies of the continuous Marangoni flow of partially miscible fluids on water [24]. The radius of the source r_s remains equal to the needle diameter until a threshold flow rate, only weakly dependent on solution formulation, is reached, after which r_s increases.

To understand the physics underlying the observed flows, we reconstructed the surface velocity field by tracking the interfacial motion of the tracers in the steady regime $r_t = r_{t,\text{max}}$ (movie M4 in the Supplemental Material [34]). The tracers moved along the radial direction only

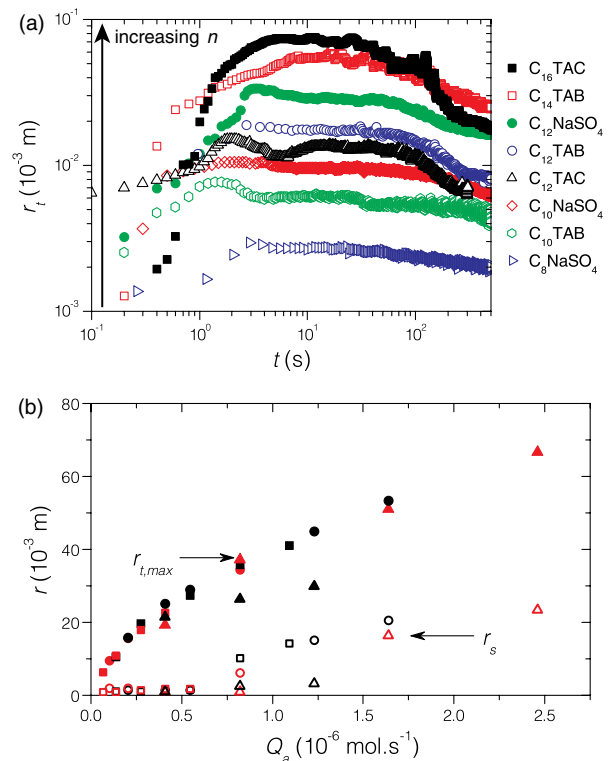


FIG. 2 (color online). Characterization of the transparent zone. (a) Radius of the transparent zone r_t as a function of time t for different surfactants. $Q_a = 0.52 \times 10^{-6} \text{ mol} \cdot \text{s}^{-1}$ for all experiments. (b) Maximum radius $r_{t,\text{max}}$ (filled symbols) and source radius r_s (open symbols) as a function of Q_a for identical amounts of $\text{C}_{12}\text{NaSO}_4$ injected in the water layer.

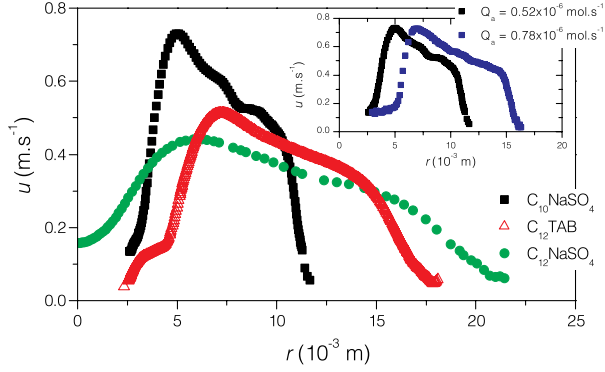


FIG. 3 (color online). Characterization of the velocity field in the transparent zone in steady state. Radial component u of the interfacial velocity field in the transparent zone as a function of the radial position r . Surfactant molar flow rate $Q_a = 0.52 \times 10^{-6} \text{ mol} \cdot \text{s}^{-1}$. Inset: velocity component u for a flow induced by $C_{10}\text{NaSO}_4$ at different flow rates Q_a .

with a velocity u whose dependence on r is similar for all the surfactants we tested (Fig. 3). When the tracers leave the source, where $u \approx 10^{-2} \text{ m} \cdot \text{s}^{-1}$, they accelerate, reach a maximum velocity $u_{\max} \approx 0.5 \text{ m} \cdot \text{s}^{-1}$, before decelerating as they travel across the transparent area. Finally, tracers decelerate abruptly as they reach $r = r_t$. The magnitude of u_{\max} decreases with an increase of n and/or r_{eff} . The injection flow rate has little effect on the velocity field (inset in Fig. 3). We note that the velocity field shapes are qualitatively similar to those reported in studies on the spreading of partially miscible fluids on water [24–26], for which partial theoretical descriptions were given.

Inspired by the similarity between velocity profiles obtained for different surfactants (Fig. 3), we plotted u/u_{\max} versus $(r - r_s)/(r_{t,\max} - r_s)$. Figure 4(a) shows that the velocity fields plotted with the rescaled coordinates collapse on a nearly universal profile. The location at which $u = u_{\max}$ is $(r - r_s)/(r_{t,\max} - r_s) \approx 0.2$ for all of the tested surfactants. The profiles have a similar slope during the deceleration stage for $(r - r_s)/(r_{t,\max} - r_s) > 0.2$.

The universality of the velocity fields suggests that a theoretical analysis in terms of scaling arguments, combining the hydrodynamics of the bulk layer and surfactant physicochemical properties, may capture the features of the flow in the transparent zone. The bulk and the interface of the layer are initially quiescent and surfactant-free. After we begin injecting surfactants, the Marangoni stress triggers a flow close to the interface, and momentum diffuses towards the bulk of the layer. In steady state, the balance between convection and diffusion results in a viscous boundary layer with thickness $\ell_v \approx (\nu r_* u_*^{-1})^{1/2}$, with $\nu = \eta/\rho$ the kinematic viscosity (i.e., the diffusion coefficient for momentum), η and ρ , respectively, the dynamic viscosity and the density of the fluid in the layer, u_* a characteristic velocity at the interface, and r_* the distance over which radial velocity gradients are established, i.e., the radius of the

flow we want to determine. We assume that surface tension gradients in regions extending to $r > r_*$ are much smaller than in the area defined by $r < r_*$, an assumption supported by previous work on continuous Marangoni flows [28].

The fluid moving along the interface advects surfactants, which desorb and diffuse towards the bulk. We assume that adsorption or desorption processes occur on time scales much shorter than surfactant diffusion in bulk water. Interface-bulk mass exchange is thus diffusion limited, and a mass transfer boundary layer grows, whose thickness scales as $\ell_c \approx (Dr_* u_*^{-1})^{1/2} = \text{Sc}^{-1/2} \ell_v$, with $\text{Sc} = \nu D^{-1}$ the Schmidt number. The expression for ℓ_c is valid if the viscous boundary layer is much larger than the mass transfer boundary layer, i.e., if $\text{Sc} \gg 1$. This condition is fulfilled in our case as, for $D \approx 10^{-10} \text{ m}^2 \cdot \text{s}^{-1}$ and $\nu = 10^{-6} \text{ m}^2 \cdot \text{s}^{-1}$ for water, $\text{Sc} \approx 10^4$. The bulk concentration thus varies from a high value just below the interface to zero at the bottom of the mass boundary layer. We choose the cmc c_* of the surfactants as the concentration scale relevant to the description of surfactant transport because of the dependence of the radius of the Marangoni flow on the properties of both the hydrophobic tail and the polar headgroup of the surfactants [Fig. 2(a)], in the spirit of Traube’s law and the hydrophilic-lipophilic balance (HLB) [21], which are key elements in the thermodynamic definition of the cmc [31–33].

Our rationale is based on the assumption that only a negligible amount of surfactants covers the water surface in the outer region compared to the water surface inside the transparent zone. At the time of measurement, surfactant bulk concentration in the water layer is a fraction of the cmc (Fig. S3 in the Supplemental Material [34]), and the amount of surfactants maintained at the interface is thus small. We neglect the latter and assume complete desorption. Hence, the surfactant mass balance can be expressed as $Q_a \propto r_*^2 D c_* \ell_c^{-1}$. Replacing ℓ_c , we find

$$Q_a \propto r_*^{3/2} (D u_*)^{1/2} c_* \quad (1)$$

Stress continuity at the air-water interface requires $\eta u_* \ell_v^{-1} \approx (\gamma_w - \gamma_s) r_*^{-1}$, with γ_w the surface tension of ultrapure water and γ_s the surface tension of the surfactant solution. From this condition, we obtain an expression for the velocity,

$$u_* = A \left(\frac{(\gamma_w - \gamma_s)^2}{\eta \rho r_*} \right)^{1/3}, \quad (2)$$

and by replacing u_* in Eq. (1) with Eq. (2), we obtain

$$r_* = B \left(\frac{\eta \rho}{(\gamma_w - \gamma_s)^2 D^3} \right)^{1/8} \left(\frac{Q_a}{c_*} \right)^{3/4}, \quad (3)$$

where A and B are two dimensionless prefactors. We estimate the values predicted for u_* and r_* with typical

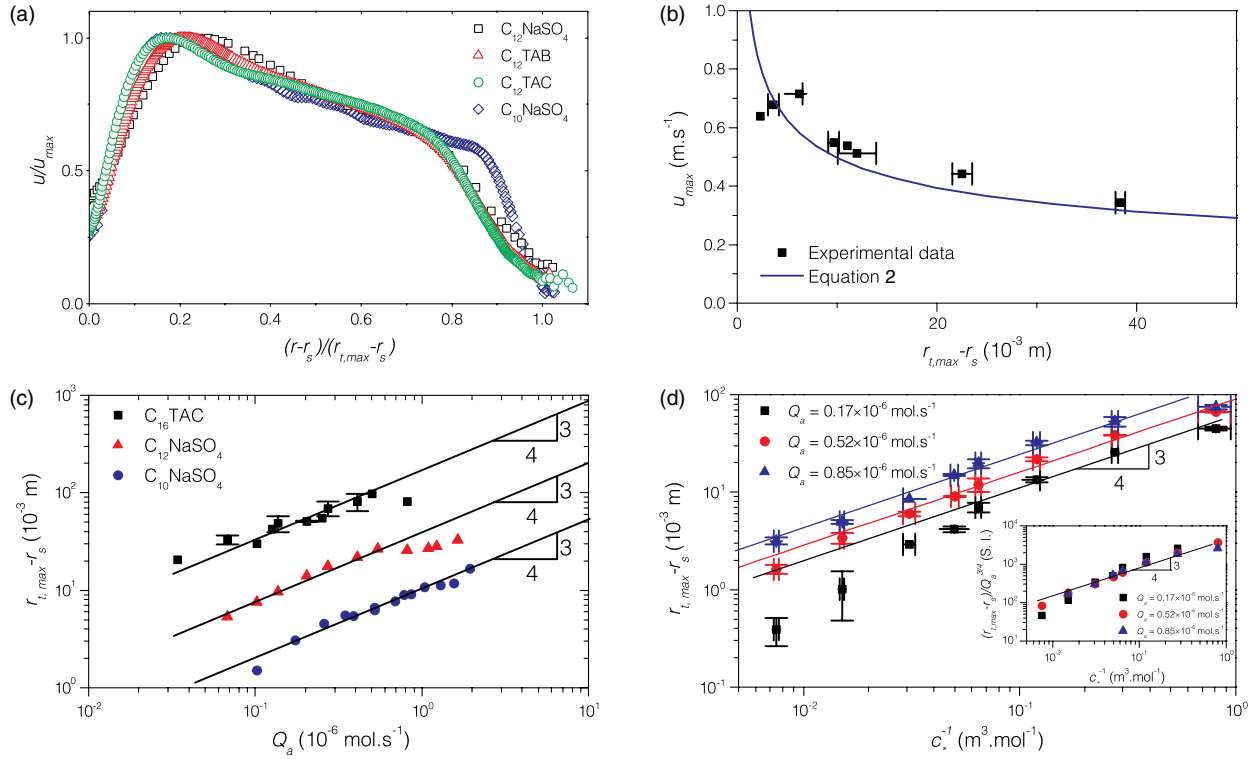


FIG. 4 (color online). Universality of the velocity field in the transparent zone in steady state and scaling laws. (a) Rescaled velocity profiles u/u_{\max} as a function of the rescaled radial coordinate $(r - r_s)/(r_t - r_s)$ for identical amounts of surfactants. (b) Comparison between Eq. (2) and experimental data for u_{\max} as a function of the maximal size of the transparent zone $r_{t,\max} - r_s$. (c) Comparison between Eq. (3) and experimental data for $r_{t,\max} - r_s$ as a function of Q_a . (d) Comparison between Eq. (3) and experimental data for $r_{t,\max} - r_s$ as a function of the inverse of the critical micellar concentration c_* . Inset: collapse of the experimental data for $r_{t,\max} - r_s$ rescaled by $Q_a^{3/4}$ as a function of c_*^{-1} . All data points were measured for the same surfactant amount in the layer, $n_s = Q_a t = 17.2 \times 10^{-6}$ mol.

values of the different parameters involved in Eqs. (2) and (3) while assuming that $c_* = 10^{-2}$ M, and $\gamma_w - \gamma_s$ is constant for all experiments and equal to $33 \text{ mN} \cdot \text{m}^{-1}$, a realistic value for the surfactant solutions we used. Setting both A and B to unity, we find $u_* \approx 0.5 \text{ m} \cdot \text{s}^{-1}$ and $r_* \approx 15 \times 10^{-3} \text{ m}$, which compare very well with our experimental findings for the maximum velocity and the radius of the flow (Fig. 3).

We compare Eq. (2) to the experimental data by taking $u_* = u_{\max}$ and $r_* = r_{t,\max} - r_s$. Figure 4(b) shows that Eq. (2) captures the experimental measurements very well, with a prefactor $A \approx 1$. This agreement supports our assumption of a constant interfacial tension difference $\gamma_w - \gamma_s$. We note that Eq. (2) fails to capture the data for surfactants forming transparent zones comparable in size to the millimeter-long meniscus connecting the needle tip to the water surface, which is not surprising since there is no length scale separation in this case.

The $3/4$ exponent in Eq. (3) is in excellent agreement with the experimental data for $r_{t,\max} - r_s$ as a function of both Q_a and c_* [Figs. 4(c), 4(d)]. The prefactor B in Eq. (3) is close to unity (see Fig. S4 in the Supplemental Material [34]). Equation (3) also collapses the experimental

data as a function of c_*^{-1} onto a master curve [inset in Fig. 4(d)]. The discrepancy between Eq. (3) and data at high flow rates in Fig. 4(c) is related to the destabilization of the source. Preliminary experiments indicate that the disagreement between data and Eq. (3) at the lowest flow rate in Fig. 4(d) results from a decrease of the magnitude of $\gamma_w - \gamma_s$. Our experiments confirm that the radius r_t of the transparent zone flow increases with an increase of the viscosity of the layer (see Fig. S5 in the Supplemental Material [34]). Thus, the test of the scaling laws against Q_a , c_* , and the viscosity of the bulk layer show that Eqs. (2) and (3) contain the appropriate physicochemical ingredients to describe Marangoni flows induced by water-soluble surfactants on water. Moreover, comparison between the scaling laws and the experimental data shows that the values of the prefactors in Eqs. (2) and (3) are close to unity, which supports the validity of the theoretical arguments. Finally, as all the surfactants we used have similar bulk diffusion coefficients D , our results establish the equilibrium cmc as a critical quantity to understand the out-of-equilibrium Marangoni flow.

Our study identifies the link between the molecular structure of hydrosoluble surfactants and the macroscopic

Marangoni flow these species induce at an air-water interface. We demonstrate that this flow has a finite extent whose magnitude is related to the critical micelle concentration of surfactants in water. We also show that the velocity field associated with the Marangoni flow has universal features, and we provide scaling laws that relate both the radius and the maximum velocity of the flow to the cmc. Our findings establish the basis for a new fast method to measure the critical micelle concentration of amphiphiles. Indeed, measuring the cmc often requires the time-consuming measurement of one property of a solution of amphiphiles such as its surface tension as a function of amphiphile concentration. In contrast, our method provides an estimate of the cmc from a single measurement of the size of the spreading area at a given flow rate, accompanied by a single independent measure of the surface tension of the solution.

The authors thank C. Breward, B. Dollet, F. Gilet, M.-C. Jullien, H. Kellay, and D. Langevin for helpful discussions. H. A. S. and M. R. thank Unilever Research for partial support of this research.

*Corresponding author.

hastone@princeton.edu

†Present address: Laboratoire de Physique des Solides, Université Paris Sud—CNRS UMR 8502, Bâtiment 510, 91405 Orsay, France.

Corresponding author.

roche.matthieu@gmail.com

‡Present address: MMN, CNRS, ESPCI Paris-Tech, 10 rue Vauquelin, 75005 Paris, France.

- [1] V. G. Levich and V. S. Krylov, *Annu. Rev. Fluid Mech.* **1**, 293 (1969).
- [2] A. H. Jobe, *N. Engl. J. Med.* **328**, 861 (1993).
- [3] J. B. Grotberg, *Annu. Rev. Fluid Mech.* **26**, 529 (1994).
- [4] R. M. Harshey, *Annu. Rev. Microbiol.* **57**, 249 (2003).
- [5] T. Eisner, M. Eisner, and M. Siegler, *Secret Weapons: Defense of Insects, Spiders, Scorpions, and Other Many-Legged Creatures* (Belknap Harvard, Cambridge, Massachusetts, and London, England, 2005).
- [6] J. W. M. Bush and D. L. Hu, *Annu. Rev. Fluid Mech.* **38**, 339 (2006).
- [7] I. B. Ivanov and P. A. Kralchevsky, *Colloids Surf., A* **128**, 155 (1997).
- [8] I. Cantat *et al.*, *Foams: Structure and Dynamics* (Oxford University Press, Oxford, 2013).
- [9] D. Quéré, *Annu. Rev. Fluid Mech.* **31**, 347 (1999).
- [10] O. K. Matar and R. V. Craster, *Phys. Fluids* **13**, 1869 (2001).
- [11] G. T. Barnes, *Agricultural Water Management* **95**, 339 (2008).
- [12] M. A. Herzig, G. T. Barnes, and I. R. Gentle, *J. Colloid Interface Sci.* **357**, 239 (2011).
- [13] D. Halpern and J. B. Grotberg, *J. Fluid Mech.* **237**, 1 (1992).
- [14] O. E. Jensen and J. B. Grotberg, *Phys. Fluids A* **5**, 58 (1993).
- [15] K. S. Lee and V. M. Starov, *J. Colloid Interface Sci.* **314**, 631 (2007).
- [16] K. S. Lee and V. M. Starov, *J. Colloid Interface Sci.* **329**, 361 (2009).
- [17] P. Mukerjee and K. J. Mysels, Critical Micelle Concentration of Aqueous Surfactant Systems, No. NSRDS-NBS-36. National Standard Reference Data System, 1971.
- [18] V. Bergeron, *Langmuir* **13**, 3474 (1997).
- [19] Y. Hayami, H. Ichikawa, A. Someya, M. Aratono, and K. Motomura, *Colloid Polym. Sci.* **276**, 595 (1998).
- [20] G. Para, E. Jarek, and P. Warszynski, *Colloids Surf., A* **261**, 65 (2005).
- [21] M. J. Rosen, *Surfactants and Interfacial Phenomena* (Wiley-Interscience, Hoboken NJ, 2004), 3rd ed.
- [22] M. Yamanaka, T. Amano, N. Ikeda, M. Aratono, and K. Motomura, *Colloid Polym. Sci.* **270**, 682 (1992).
- [23] M. T. Yacilla, K. L. Herrington, L. L. Brasher, E. W. Kaler, S. Chiruvolu, and J. A. Zasadzinski, *J. Phys. Chem.* **100**, 5874 (1996).
- [24] D. G. Suciu, O. Smigelschi, and E. Ruckenstein, *AIChE J.* **13**, 1120 (1967).
- [25] D. G. Suciu, O. Smigelschi, and E. Ruckenstein, *AIChE J.* **15**, 686 (1969).
- [26] D. G. Suciu, O. Smigelschi, and E. Ruckenstein, *J. Colloid Interface Sci.* **33**, 520 (1970).
- [27] A. Mizev, *Phys. Fluids* **17**, 122107 (2005).
- [28] N. M. Kovalchuk and D. Vollhardt, *Adv. Colloid Interface Sci.* **120**, 1 (2006).
- [29] A. Mizev, A. Trofimenko, D. Schwabe, and A. Viviani, *Eur. Phys. J. Spec. Top.* **219**, 89 (2013).
- [30] K. D. Collins, *Methods* **34**, 300 (2004).
- [31] L. Moreira and A. Firoozabadi, *Langmuir* **26**, 15 177 (2010).
- [32] I. B. Ivanov, K. G. Marinova, K. D. Danov, D. Dimitrova, K. P. Ananthapadmanabhan, and A. Lips, *Adv. Colloid Interface Sci.* **134–135**, 105 (2007).
- [33] C. Tanford, *The Hydrophobic Effect: Formation of Micelles and Biological Membranes* (Wiley-Interscience, New York, 1980), 2nd ed.
- [34] See Supplemental Material at <http://link.aps.org/supplemental/10.1103/PhysRevLett.112.208302> for a table listing the properties of the surfactants, movies of the experiments showing two experiments with water covered in pepper grains and the flow at large and small scale, a discussion on the passiveness of tracers, information on the influence of tracer packing, the evolution of the size of the flow as a function of surfactant concentration in the bulk, the effect of viscosity, information on the measurement of the velocity field, and a discussion of the magnitude of the prefactors in the scaling law.